SSRG International Journal of Civil Engineering
ISSN: 2348-8352/ https://doi.org/10.14445/23488352/IJCE-V13I6P108

Volume 13 Issue 6, 102-116, June 2026

Original Article

Physics-Informed Mesh Optimization for Improving Computational Efficiency in Urban CFD Simulations

Shubham Kumar Verma[1], Rachit Manchanda[2], Rupesh Gupta[3], Abhijit Bhowmik[4,5], Sanjay Kumar[6], Vinod Balmiki[7]

[1]*Marwadi University Research Centre, Department of Mechanical Engineering, Marwadi University, Rajkot, Gujarat, India.*
[2]*Department of Computer Science Engineering, Chandigarh University, Mohali, Punjab, India.*
[3]*Chitkara University Institute of Engineering and Technology, Chitkara University, Punjab, India.*
[4]*Department of Additive Manufacturing, Mechanical Engineering, SIMATS, Saveetha Institute of Medical and Technical Sciences, Thandalam, Chennai, India.*
[5]*Division of Research and Development, Lovely Professional University, Phagwara, Punjab, India.*
[6]*Department of Mechanical Engineering, Noida Institute of Engineering & Technology, Greater Noida, India.*
[7]*Department of Civil Engineering, Uttaranchal Institute of Technology, Uttaranchal University, Uttarakhand, India.*

[1]*Corresponding Author : sverma4585@gmail.com*

Received: 10 March 2026 Revised: 09 April 2026 Accepted: 08 May 2026 Published: 30 June 2026

Abstract *- Computational fluid dynamics (CFD) is extensively utilized to assess the thermal behaviour of pedestrians and mitigate the effects of the urban heat island. However, such analysis are usually computationally intensive and thus limit their applicability in large-scale parametric analysis. From the green computing perspective, achieving accurate and precise results at a lower cost is considered essential. However, this aspect remains underexplored in urban CFD literature. This paper tries to fill this gap by examining how mesh structure can affect thermal accuracy and computing efficiency. The test case of this study is a hypothetical urban domain which is consisted of a 3x3 array of buildings. The study tested six mesh configurations to understand their effects. Thermal accuracy is measured by the pedestrian level canyon-averaged air temperature and the measures of evaluating computational efficiency are solver convergence behaviour and wall-clock time. A Mesh Performance Index (MPI) is proposed to enable the combined effect of both the thermal precision and the computational expense in order to support the integrated evaluation. The findings indicate that uniformly refined meshes increase computational cost without improving convergence or thermal accuracy, whereas coarse meshes reduce runtime but fail to adequately solve the pedestrian-level thermal gradients. Conversely, the optimized mesh achieved a thermal accuracy close to baseline at a reduction of about 74 percent in wall-clock time over the physics-informed mesh. Not only this, but optimized mesh has also listed MPI values which are 1.8 to 178.5 times higher than that of the other configurations. These findings suggest that optimization of mesh using physics can be used to considerably reduce the energy requirement and preserve the thermal fidelity. This method offers a viable way to more environmentally friendly and sustainable urban CFD simulations.*

Keywords *- Computational fluid dynamics, Energy efficiency, Mesh optimization, Pedestrian behaviour, Urban microclimate.*

1. Introduction

Rapid population and economic growth have driven increased migration from rural to urban areas, thereby resulting in accelerated global urbanization [1]. Due to this growth, natural surfaces are being substituted with artificial ones, such as concrete, asphalt, and buildings [2-4]. This change alters the city's thermal environment and leads to the Urban Heat Island (UHI) [4]. The UHI effects refers to the phenomenon where temperatures in cities are higher compared to the surrounding rural areas. [5, 6] This effect increases ambient temperatures, decreases pedestrian comfort, and increases energy demands [7-9]. High-density regions may limit air circulation and trap heat in street canyons, thereby resulting in intensified local heat stress [10]. These conditions are particularly critical in hot climates, where low winds can significantly affect thermal perception and cooling energy demand. These processes are critical to understand and are therefore essential for designing climate-resilient and energy-efficient urban environments. These challenges highlight the need for a better understanding of urban microclimates and their interactions with urban form.

Urban microclimate modelling has been considered as an important method for examining the airflow, heat transfer, and thermal conditions in complex urban microclimates [11, 12]. Among the various available approaches, Computational

Fluid Dynamics (CFD) is extensively utilized to conduct detailed airflow and heat transfer analysis. Many studies have shown that CFD can accurately simulate pedestrian wind flow and thermal conditions, which can be useful for urban planning and heat mitigation strategies. For instance, Melani et al. [13] demonstrated that multi-scale CFD modelling can effectively capture pedestrian wind conditions by coupling regional atmospheric flow with building-scale simulations. In a similar study, Silva et al. [14] studied the effects of wind direction and building height on the pedestrian behaviour and pointed out the critical importance of the configuration of the city in order to keep the outdoor comfort.

In the context of heat mitigation strategies, Zeeshan and Ali [15] investigated the effects of cool materials, greenery and water bodies and found a notable enhancement in thermal comfort. Similarly, Author studied the influence of reflective pavements and green infrastructure on microclimate. They found average temperature reduction of 0.16-0.33℃ across the different strategies. Furthermore, Cao and Li [16] studied the spatial form effect on urban wind environment. They noted that optimal building planning can decrease the stagnant wind areas and pedestrian comfort.

Chew et al. [17] also showed that passive ventilation measures can optimize the ventilation in urban street canyons and improve pedestrian-level thermal conditions in warm climates. More recently, CFD simulation was used to study the effect of morphology and void-integrated building design on wind power density and turbulence by Yang et al. [18] Meanwhile, Author emphasized the need to incorporate PCM to enhance the thermal performance of indoor environment.

Nevertheless, these improvements have not yet been sufficient to make CFD predictions reliable enough to be independent of modelling assumptions and discretization methods. The resolution of the mesh is believed to play a key role in flow and thermal field simulation accuracy. Several studies have emphasized the importance of grid convergence and mesh sensitivity analysis in ensuring reliable CFD predictions [19]. Insufficient mesh resolution may result in under-resolved boundary layers and/or distorted recirculation patterns and incorrect thermal predictions [19, 20]. On the other hand, excessively refined meshes may lead to a large but disproportionate increase in computational cost without any significant improvement in accuracy[20].

Previous studies indicate that in some urban flow scenarios medium grid resolutions can be used to obtain results similar to those obtained in finer resolutions [19, 21] and the grid convergence method, such as the one validated by Li et al. [22] can provide a systematic approach to ensure solution reliability. The results underscore the importance of mesh design in attaining the balance between effort and accuracy. The resolution of the meshes has also been found to be one of the important factors that affects the modeling error in urban airflow and thermal simulations [23]. It directly influences the velocity field prediction, the turbulence characteristics and thermal gradients of the street canyon and the buildings [24-26]. High-fidelity approaches like Large Eddy Simulation (LES) require even more stringent mesh resolutions to resolve near-wall turbulence and wake interactions [27]. Further research work on pedestrian wind comfort and pollutant dispersion has demonstrated that when the mesh is not designed properly, the behaviour of the flow can be significantly different from what is predicted [22, 27-31]. It was also apparent from the urban modelling studies that it is important to design the grid and carry out appropriate validation procedures to ensure accurate modelling [32, 33]. These results demonstrate the significance of the proper design of the mesh and sensitivity analysis in the CFD simulation of urban flows.

To address these challenges, hybrid and non-uniform meshing methods have been proposed to resolve the need to focus the resolution on the building surfaces and pedestrian areas, while relaxing in less critical areas. Also, the extrusion-exclusion discretization technique is another useful strategy to reduce meshing time and effort [34]. In broader CFD research, adaptive and physics-based mesh refinement methods have also been developed that allow the grids to dynamically or strategically adapt to flow features to improve numerical efficiency without sacrificing solution accuracy [35, 36]. At the same time, researchers have been focused on the trade off between the effort, cost and accuracy of the solution [37, 38], with excessive mesh refinement causing significant computational overhead.

A data-driven approach also has been developed in recent years as a viable alternative to enhance CFD efficiency and mesh design [39, 40]. Machine learning (ML) techniques enables faster evaluation of flow behaviour while reducing computational expense [41]. For instance, a recent work has introduced ML-based frameworks that provide spatial feedback on mesh convergence by identifying regions requiring refinement using clustering-based approaches, thereby offering a more systematic alternative to traditional mesh sensitivity studies [42, 43]. The methods take advantage of features in the flow field to determine regions of interest and help to direct mesh refinement.

Additionally, ML methods have shown great promise in fields such as surrogate modelling, coarse-grid error correction, and solver acceleration, which helps to save computational time and enhance workflow efficiency [41, 44]. However, these strategies are typically data-driven, feature engineered, and problem-specific tuned, which can restrict the generalizability and physical interpretability of these approaches. In addition, as noted in recent studies, mesh generation in practice still relies heavily on user experience and heuristic decisions, and systematic frameworks for evaluating mesh performance remain limited.

In parallel, high-performance computing techniques such as parallel processing and GPU acceleration have been widely used to reduce simulation runtime [45, 46]. Although these methods improve computational throughput, they do not address the numerical efficiency of mesh design itself, which remains a key factor governing overall simulation performance. In other areas of computational science, the energy consumed by simulations and the resulting energy-to-solution have increasingly emerged as important metrics for sustainable computing [47-49]. However, this perspective remains scantly available in urban microclimate modelling literature, where long runtimes, excessive iteration counts, and non-converged simulations are frequently encountered without explicit consideration of their computational or energy implications [50, 51]. Consequently, limited emphasis has been placed on developing mesh design strategies that simultaneously address numerical accuracy, computational efficiency, and sustainability in urban CFD applications.

Collectively, literature on urban CFD studies can therefore be roughly categorised into three areas: (i) urban airflow and thermal environment assessment, (ii) mesh sensitivity and grid convergence analysis, and (iii) computational acceleration and data-driven methods. However, these approaches typically address accuracy, computational speed, or data-driven enhancement independently. There is no systematic framework that combines design of the mesh, thermal accuracy and computational efficiency into a single evaluation framework. This is especially important compared to emerging AI/ML-based methods that focus primarily on refinement or acceleration rather than on integrated performance assessment.

This gap highlights the need to reframe mesh design as a performance-driven, sustainability-oriented decision that balances computational cost and solution accuracy. This study examines the influence of different mesh configurations on solver convergence, pedestrian-level thermal accuracy, and computational cost in urban CFD simulations. The main novelty of this work lies in explicitly linking mesh design to computational efficiency by introducing a Mesh Performance Index (MPI) that integrates prediction accuracy and computational cost into a single quantitative metric.

The proposed framework uses a physics-informed mesh optimization method, which is different from other methods of uniform refinement or heuristic mesh selection, or data-driven training. The study systematically evaluates multiple mesh configurations within a controlled urban domain and demonstrates that targeted mesh optimization can achieve near-baseline thermal accuracy with a substantial reduction in computational cost. This provides a robust and interpretable framework for improving computational efficiency while maintaining physical reliability in urban CFD simulations. The primary goals of this study are:

- To evaluate the influence of different mesh configurations on solver convergence and computational cost.
- To assess pedestrian-level thermal accuracy using canyon-averaged air temperature.
- To quantify the trade-off between computational efficiency and thermal accuracy.
- To develop and apply a Mesh Performance Index (MPI) for integrated performance evaluation.

2. Methodology

This section describes the methodological framework used in the study. It consists of five successive stages as illustrated in Figure 1. It starts from the development of model. This involves creating a geometric model, meshing, finalising governing equations, and setting up boundary conditions and numerical parameters.

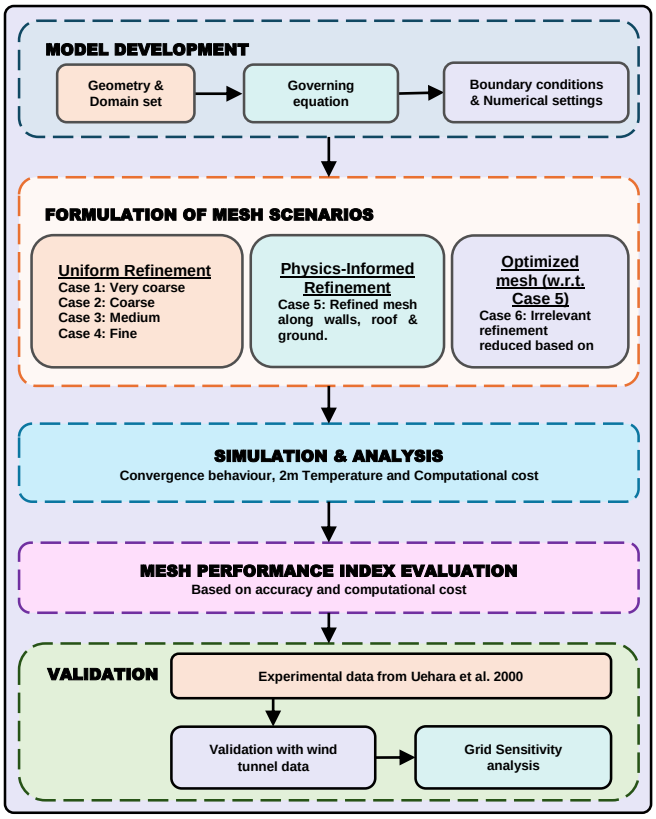

Fig. 1 Methodological framework adopted in the present study

Subsequently, multiple mesh refinement scenarios are formulated and systematically evaluated. This followed by the numerical simulation. Based on the simulations, performance will be assessed through convergence behaviour, pedestrian-level air temperature, and computational cost. Thereafter, the obtained results were utilized for quantifying the Mesh Performance Index (MPI). Finally, model validation is carried out using a sensitivity analysis of grid and the comparison of results with benchmark experimental results. The validation simulations employ the same meshing strategy as the

optimized configuration, but the geometry and mesh resolution are scaled to match the experimental setup.

2.1. Urban Domain

To examine the influence of mesh design on urban modelling accuracy and computational effort, a hypothetical urban domain consisting of nine buildings (arranged in a 3×3 array) is considered. Each building is assumed to have a plan dimension of 5m×5m, with a height to width ratio of 1. The inner building spacing is maintained at 5 m in both streamwise and spanwise directions. This configuration results in twelve street canyons and is commonly adopted in urban CFD studies to investigate pedestrian-scale thermal environments. The buildings are considered to be situated in typical climatic conditions in Rajkot, Gujarat, India. To minimize boundary effects and ensure proper development of flow and thermal fields, the geometry of the domain is extended 15H in lateral directions and 5H in the upward direction, consistent with established urban CFD best-practice guidelines [52]. A graphical representation of the urban domain considered for study is shown in Figure 2. It highlights the top view, front view and a three-dimensional view of the urban domain.

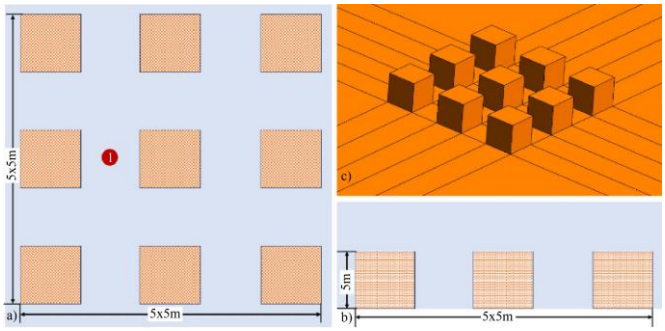

Fig. 2 Schematic layout showing a) Top view, b) Side view & c) Three-dimensional (3D) layout of domain taken up for study.

2.2. Numerical Set Up

To model the airflow distribution within the computational domain, a 3D CFD based urban microclimate model is employed. The numerical framework employed in this study is based on a previously validated computational setup, as reported in Author Studies where the model was extensively verified and validated against experimental and numerical datasets. This ensures the reliability of the governing equations, turbulence modelling approach, and numerical schemes used in the present work.

The model enables detailed analysis of airflow patterns, convective heat transfer, and temperature distribution within the urban environment. A steady-state Reynolds-averaged Navier-Stokes equation is numerically solved to understand the flow distribution. The energy equation is integrated with the momentum equations to evaluate thermal behaviour within the domain. The buoyancy effects arising from temperature gradients are incorporated by using the Boussinesq approximation. The governing equations adopted are presented in Equations (1)-(3).

$$\frac{\partial U_i}{\partial x_i} = 0 \tag{1}$$

$$U_j \frac{\partial U_i}{\partial x_j} = -\frac{\partial P}{\partial x_i} + (\nu + \nu_t)\frac{\partial}{\partial x_j}\frac{\partial U_i}{\partial x_j} - \beta\left(T - T_{ref}\right)g_i \tag{2}$$

$$U_i \frac{\partial T}{\partial x_i} = (\alpha + \alpha_t)\frac{\partial^2 T}{\partial x_i^2} \tag{3}$$

Here, U_i denotes i^{th} component of velocity, and P represents the kinematic pressure. The air temperature is represented by T, and T_{ref} denotes the reference air temperature. Subsequently, the kinematic viscosity of the air (ν) is taken as 1.0×10^{-5} m^2s^{-1}, while the turbulent viscosity, ν_t is computed with the help of the k-epsilon turbulence model. β (K^{-1}) denotes a thermal expansion coefficient of air and g_i represents the gravitational acceleration component in the i^{th} direction. Thermal transport is modelled using thermal diffusivity (α) which is computed as $\alpha = \frac{\nu}{Pr}$, where Pr represents Prandtl number. Subsequently, α_t denotes a turbulent thermal diffusivity, while the air density is assumed to be 1.0 kg/m^3 at temperature T.

Despite the use of a previously validated numerical framework, additional verification and validation are necessary due to differences in mesh configuration and domain discretization implemented in the present study. Therefore, this study verifies the results obtained from the optimized mesh configuration through a grid independence study and validates the simulation results against experimental results of thereby ensuring the numerical reliability of the discretization and the physical reliability of the model predictions.

2.3. Different Scenarios

To assess the impact of mesh resolution and structure on numerical accuracy and computational efficiency, six different mesh configurations are developed for the same urban domain. The meshing process begins with the generation of a two-dimensional (2D) structured mesh on a horizontal plane of the modelled domain. This base mesh is subsequently extruded vertically using the extrusion-exclusion discretization method, which is proposed by van Hooff and Blocken [34]. In this, a 2D mesh is extended vertically to form a structured 3D grid. The solid building volumes are then discarded from the extruded mesh, leaving a high quality hexahedral mesh of the fluid domain.

The six mesh configurations developed for the assessment span from uniformly coarse to optimized non-uniform strategies for refinement. These configurations are set up to systematically study the balance between computational cost and the accuracy of the solutions. For Cases 1 and 2, uniform refinement is made across the computational domain to serve as a reference case for the mesh behaviour as the global resolution is gradually increased. For Cases 3 and 4, further

refinement is added to the building regions to capture finer-scale separation, wake and thermal recirculation regions, which are often found near urban buildings.

Case 5 uses a physics-informed mesh refinement strategy as described by Author, where the high resolution meshes are focused around walls, roofs, ground surfaces and street canyons where the velocity and thermal gradients are likely to be high. These regions are associated with near-wall boundary layer development, buoyancy-induced thermal stratification, pedestrian-level heat accumulation, and vortex formation, all of which significantly influence urban thermal behaviour.This will allow the mesh to accurately capture the dominant flow and heat-transfer mechanisms while avoiding unnecessary refinement in relatively uniform regions of the domain.

Based on this physics-informed refinement approach, Case 6 is developed by selectively decreasing element density in places where the impacts on the temperature distribution and flow behaviour are not as great. This approach will maintain thermal prediction accuracy with minimal computational costs and to maximize the overall numerical efficiency. Figure 3(a-f) illustrates the different mesh configurations adopted in the study, while the corresponding mesh characteristics, element counts, and mesh types are summarized in Table 1.

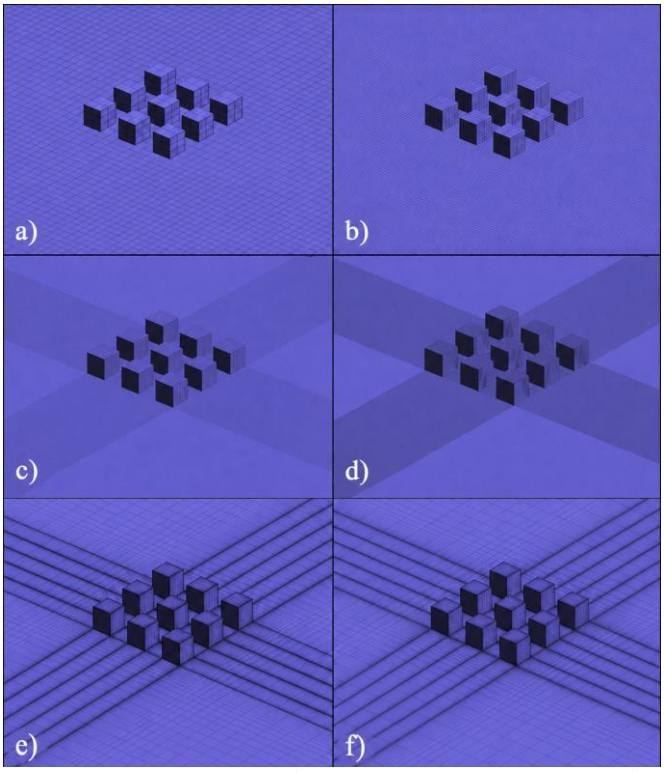

Fig. 3 Computational mesh configurations used in the present study for Cases 1-6

Table 1. Various mesh configurations considered for the study

Scenario	Mesh size	Refinement strategy	No of elements	Element type
Case 1	Very coarse	Uniform	112788	Structured hexahedral
Case 2	Coarse	Uniform	776804	Structured hexahedral
Case 3	Medium	Uniform	1483160	Structured hexahedral
Case 4	Fine	Uniform	2770620	Structured hexahedral
Case 5	Physics-informed	Non-uniform	1723580	Structured hexahedral
Case 6	Optimized	Optimized	711504	Structured hexahedral

2.4. Boundary Conditions

To conduct these simulations, a representative hot-day scenario is considered, with a reference ambient air temperature of 312 K. The wind speed at the inlet is set at 1 m/s to represent low ventilation (high pedestrian level thermal stress). This is achieved by using a velocity inlet condition at the inlet. The inlet turbulence quantities are specified using standard atmospheric boundary layer formulations given in Equations (4)-(5):

$$k(z) = \frac{(u_*)^2}{\sqrt{C_\mu}} \quad (4)$$

$$\epsilon(z) = \frac{(u_*)^3}{\kappa(z+z_0)} \quad (5)$$

Here u_* represents friction velocity, C_μ denotes model constant of the k-epsilon turbulence model, κ is taken as 0.41 which represents the von Karman constant, and Z_0 (taken as 1m) represents the aerodynamic roughness length.

Subsequently, a zero gradient boundary condition is used for downstream boundary to ensure numerical stability. The top boundary is considered to be a symmetry boundary to prevent artificial shear effects. No-slip boundary conditions for velocity are given to all solid surfaces, such as building walls and roofs, or the ground. The temperature on all solid surfaces is kept at a uniform value of 315 K, based on preliminary estimates and is representative of heated urban surfaces during hot days. It is relevant to mention that all the mesh configurations use the same domain geometry, equations, numerical scheme and boundary conditions. So if there is any difference observed in the convergence behaviour or thermal prediction or computational costs, this can only be attributed to differences in the design of the mesh.

2.5. Evaluation Metrics

Thermal accuracy, solver behaviour and computational efficiency are used as three key metrics to evaluate the performance of the various mesh configurations. Pedestrian level air temperature (2m) is used to evaluate thermal accuracy. This included measuring the average temperature of the canyons (T_c) in each street canyon. The 3x3 building

configuration creates 12 street canyons, each of which is an independent unit for evaluation. The canyon-averaged temperature is generally used as the main accuracy measure because it offers a physically meaningful representation of the thermal conditions to which pedestrians are exposed and is less sensitive to the numerical variations in the model in a specific location.

The performance of the solver is measured by convergence behaviour, number of iterations and wall-clock time. The wall-clock time is used as a practical indicator of energy-to-solution, as all simulations are performed using identical numerical settings on the same computational platform. To enable a combined assessment of thermal accuracy and computational efficiency, a Mesh Performance Index (MPI) is introduced. It is primarily dependent on the accuracy index and the computational cost index. The physics-informed mesh configuration (Case 5) is treated as the baseline for relative comparison. The Accuracy Index (AI) for a given mesh configuration i is defined using the percentage deviation of canyon-averaged temperature from the baseline:

$$AI_i = \frac{|\overline{T}_{c,i} - \overline{T}_{c,b}|}{\overline{T}_{c,b}} \times 100 \quad (6)$$

Here $\overline{T}_{c,i}$ represents canyon-averaged temperature for mesh, and $\overline{T}_{c,b}$ denotes the corresponding value for the baseline mesh.

The computational Cost Index (CI) is defined using wall-clock time as detailed in Equation (7):

$$CI_i = \frac{t_i}{t_b} \quad (7)$$

where t_i is the wall clock time for mesh and t_b is the wall-clock time for the baseline mesh.

The overall Mesh Performance Index (MPI) is then expressed using Equation (8) as:

$$MPI_i = \frac{1}{\lambda_A AI_i + \lambda_C CI_i} \quad (8)$$

Where λ_A and λ_B are weighting factors assigned to accuracy and computational cost, respectively. In this study, greater importance is assigned to thermal accuracy by setting $\lambda_A = 0.75$ and $\lambda_C = 0.25$. A higher MPI value indicates a more favourable balance between pedestrian-level thermal accuracy and computational efficiency relative to the baseline configuration.

3. Results and Discussion

3.1. Solver Convergence and Computational Cost

The solver convergence behaviour and computational cost for all mesh configurations are examined to establish numerical feasibility and energy-to-solution characteristics prior to analysing thermal results. The convergence is evaluated based on residual reduction and stabilization of air temperature, while computational cost is quantified using wall-clock time. In order to have a fair and conservative evaluation of solver behaviour in all mesh configurations, relaxed convergence criteria are employed. The pressure residual convergence criterion is set to 10^{-2}, and the remaining governing equations are controlled with a convergence tolerance of 10^{-3}. These criteria are applied consistently across all the cases. Despite this generous tolerance, several mesh configurations fail to achieve stable residual decay, which is an indication of numerical inefficiency associated with excessive or poorly structured mesh refinement. Figure 4(a-f) shows the convergence residual plotting of all six mesh configurations, where residuals of velocity components, pressure, turbulence quantities and enthalpy (energy equation) are plotted against the iteration number.

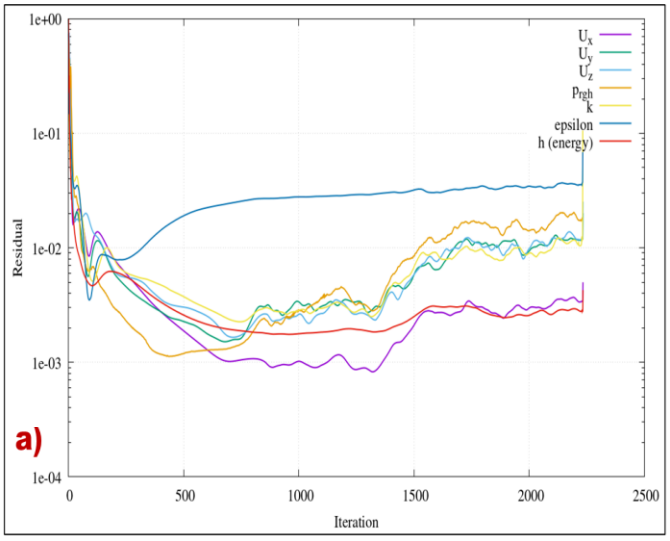

(a)

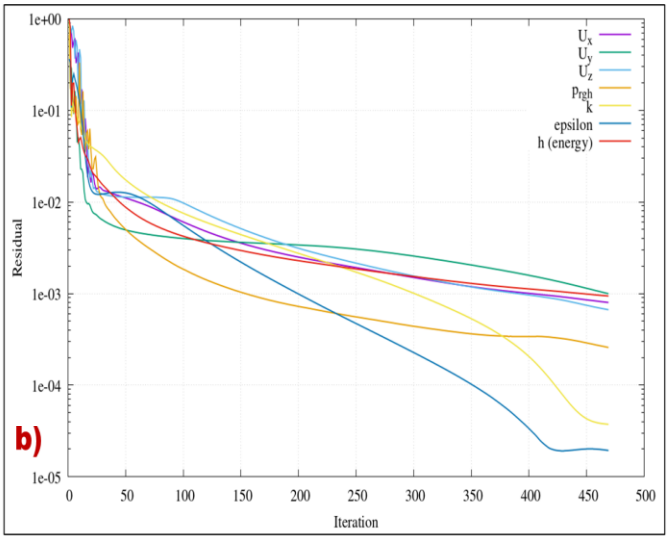

(b)

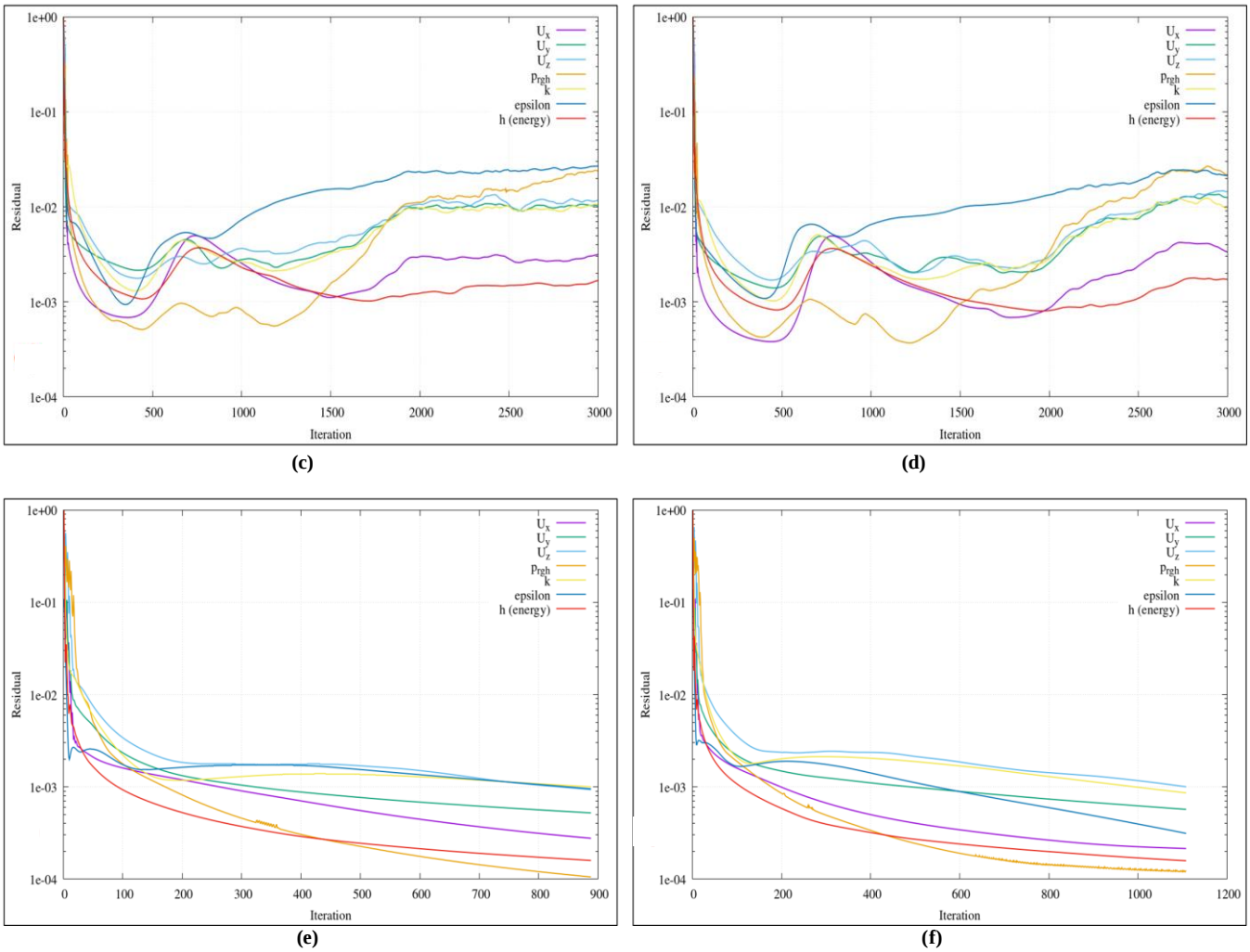

Fig. 4 Residual plot for velocity, pressure, turbulence and enthalpy for Cases 1-6

The very coarse mesh (Case 1, Figure 4a) exhibits irregular residual behaviour with observable oscillations after the initial decay phase. Although some residuals temporarily reduced below the prescribed thresholds, they subsequently fluctuate and fail to stabilize. This behaviour indicates under-resolution of flow and thermal gradients, which is further reflected in non-physical temperature predictions. Although this configuration has a low computational cost because of the limited number of elements, it proved to be physically unreliable and was not discussed any further in quantitative analysis.

Case 2 (coarse mesh, Figure 4b) is a representation of rapid and monotonic decay of the residue. All the governing equations converge to the set criteria within 469 iterations and approximately 400 seconds of clock time. There is no oscillatory behaviour in residual stabilization and the numeric robustness is good. However, its relatively coarse spatial resolution necessitates further assessment of thermal accuracy, which is examined in subsequent sections.

The medium (Case 3, Figure 4c) and fine (Case 4, Figure 4d) uniform meshes exhibit slow residual decay followed by persistent oscillatory behaviour. Though at the beginning of the iterations, the residuals are on the decline, they do not stabilize within the given 3000 iteration limit. Oscillations in the pressure and turbulence residuals are also continued and gradual increments in some components of momentum are also observed.

The computational cost of these cases is around 9303 seconds and 23866 seconds, respectively, which can be considered as significantly high in comparison to other cases. Although additional refinement could potentially improve stability, such an approach would significantly increase computational expense without guaranteeing convergence. The above observations suggest that mesh density in itself is not enough to guarantee numerical robustness and refinement strategy is a key factor with regard to solver stability. To avoid excessive computational energy consumption, both simulations were stopped after 3000 iterations.

In Case 5, a physics-based refinement strategy is used subsequently. This entails mesh refinement in areas near walls and roofs where high velocity and thermal gradients are expected. Such a setup demonstrates a smooth and steady decrease of the residual (Figure 4e), and all governing equations converged to the desired convergence criterion in about 888 iterations and 3078 wall-clock seconds.

The targeted refinement increases numerical stability with respect to uniformly refined meshes, but keeps the same physically meaningful resolution. On the basis of the results gained with the physics-informed mesh (Case 5), another attempt has been made to save computational effort by mesh optimization (Case 6). This means that less refinement is applied in areas that do not significantly affect the scores in the metrics. As a result, approximately 60% elements are reduced in comparison to Case 5.

The optimized mesh (Figure 4f) has stable and monotonic residual decay. Although it has a larger number of iterations (1108) for the convergence, it is converged in nearly one-fourth of the wall clock time of Case 5 (approx. 807 seconds) because of the fewer number of elements. The result shows that iterations are not a good enough measure of computational efficiency, and highlights the significance of considering energy to solution in green computing-related CFD studies. A summary of solver convergence behaviour and computational cost for all mesh configurations is provided in Table 2.

Table 2. Convergence behaviour and runtime for all mesh cases.

Scenario	Iterations	Clock time(s)	Convergence status
Case 1	2232	154	Diverged
Case 2	469	400	Converged
Case 3	3000	9303	Not converged
Case 4	3000	23866	Not converged
Case 5	888	3078	Converged
Case 6	1108	807	Converged

3.2. Pedestrian-Level Thermal behaviour

To evaluate pedestrian-level thermal behaviour, the air temperature at 2 m above the canopy is considered. It is considered representative of human thermal exposure in urban environments. The temperature data at each node are extracted from the urban domain. Inter-mesh comparison is carried out in terms of aggregated canyon-average metrics obtained using the extracted datasets.

In addition to quantitative analysis, spatial temperature distributions at 2 m height are examined using contour plots to assess the physical consistency of the simulated thermal fields. Although thermal quantities are evaluated for all mesh configurations, only converged and physically consistent cases are considered suitable for qualitative interpretation of contours. The absolute temperature difference and percentage error are determined with reference to the physics-informed mesh (Case 5), which is assumed to be the reference configuration in the evaluation of thermal accuracy.

The very coarse mesh (Case 1) fails to converge and produces unrealistically high canyon-averaged temperatures, with a mean value of 51.12℃ and large spatial variability (standard deviation of 2.32℃). This corresponds to an absolute deviation of 12.15℃ (approximately 31.18%) relative to the baseline, clearly indicating severely under-resolved flow and thermal physics. Although these values are reported for completeness, temperature contours for this case are not presented, as they would not represent physically meaningful pedestrian-level thermal conditions.

The coarse mesh (Case 2) produces a numerically stable solution with a mean canyon-averaged temperature of 39.43℃ and very low spatial variability (0.04 ℃). The corresponding 2 m air temperature contours are smooth yet excessively uniform, which means that the near-wall and canyon-scale thermal gradients are not sufficiently resolved (Figure 5). This under-resolution leads to a +0.46℃ deviation (1.18%) relative to the baseline, which indicates that uniform coarse discretization is inadequate for capturing pedestrian-level thermal variations.

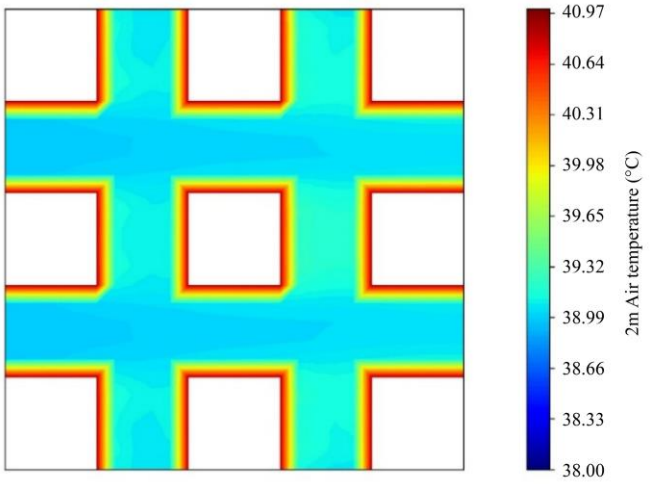

Fig. 5 Variations in 2m air temperature for Case 2.

Subsequently, the medium mesh (Case 3) and the fine mesh (Case 4) fail to converge within the prescribed iteration limits. In case 3, the averaged temperature of the canyons relative to the baseline is found to be 40.44℃ with a significant variability and deviations of 0.50℃ and 1.47℃ (3.77%), respectively. Case 4 exhibits a mean temperature of 39.55℃ and standard deviation of 0.36 ℃, thereby resulting in a deviation of +0.58 ℃ (1.49 %). Although the mesh resolution is increased, both cases become numerically unstable and their solutions are thus excluded from contour-based qualitative analysis.

The physics-informed mesh (Case 5) yields the lowest averaged temperature of 38.97℃ across canyons with a spatial variation of approximately 0.02℃. The 2m canopy level temperature contours are shown in Figure 6(a). They exhibit

consistently high thermal gradients near the wall, while other areas exhibit almost uniform and slightly lower temperature distributions, except for a few street canyons. Due to its numerical stability and physical reliability, this configuration is considered as the baseline scenario for thermal accuracy assessment. Further optimization of the mesh (Case 6) closely reproduces the baseline thermal behaviour. However, it yielded a mean canyon-averaged temperature of 39.01 ℃ and a standard deviation of approximately 0.03 ℃. The absolute difference relative to the baseline is only 0.04 °C, which has a percentage error of approximately 0.10%. Notably, 2 m temperature contours represented in Figure 6(b) are very close to the ones in the physics-informed mesh, which proves that the main pedestrian-related thermal structures are maintained even when the mesh density has decreased significantly.

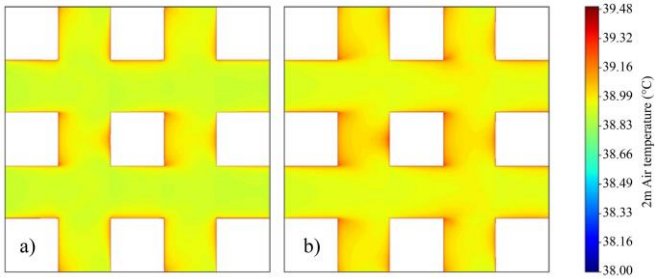

Fig. 6 Variations in 2m air temperature for a) Case 5 & b) Case 6.

Although the air temperature is evaluated separately in the twelve street canyons, findings are presented using aggregated canyon-based metrics. This method offers a physically significant and robust inter-mesh comparison framework and suppresses sensitivity to local numerical variations. This kind of representation is appropriate for the present study, which focuses on mesh efficiency and green computing considerations rather than detailed canyon-to-canyon variability. All the mesh configurations, along with their quantitative temperature-averaged statistics, are summarized in Table 3.

Table 3. Canyon-averaged pedestrian-level air temperature statistics and deviation relative to baseline

Scenario	Mean canyon temperature (℃)	Standard deviation (℃)	Temperature difference (ΔT)	Error (%)
1	51.12	2.32	+12.15	+31.18
2	39.43	0.04	+0.46	+1.18
3	40.44	0.50	+1.47	+3.77
4	39.55	0.36	+0.58	+1.49
5	38.97	0.02	0.00	0.00
6	39.01	0.03	+0.04	+0.10

3.3. Mesh Performance Index

The Mesh Performance Index (MPI) is a performance metric that compares the overall output of various mesh configurations, both in terms of thermal accuracy and computational efficiency. As detailed in the methodology section, the MPI formulation utilizes the percentage error in canyon-averaged temperature as the accuracy index and the normalized wall-clock time as the cost of computational index. The MPI obtained for all mesh configurations is shown in Figure 7.

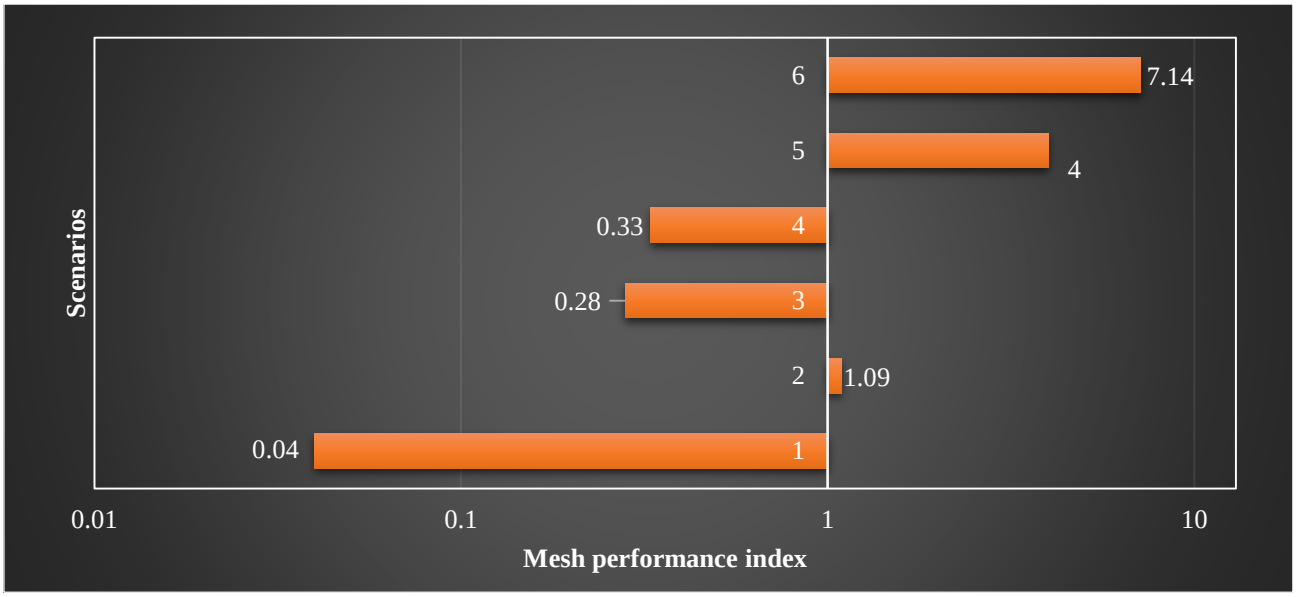

Fig. 7 MPI comparison for all mesh configurations.

The very coarse mesh (Case 1) reported a negligible MPI (0.04). This is mainly due to its large thermal error (31.18%), which may be due to unconverged simulations. This exemplifies the fact that the excessively coarse mesh can lead to physically unreliable solutions despite low computational cost. Cases 3 and 4 with medium and fine meshes also have

reported low values of MPI (0.28 and 0.33, respectively). These cases are marked with the high computational cost and non-convergence, which proves that uniform mesh refinement is not an efficient way to find an accuracy-cost trade-off in CFD simulations.

The coarse mesh (Case 2) has a moderate value of MPI (1.09). This might be a result of its minimal computing cost. But its thermal deviation of 1.18% means that it does not resolve thermal gradients at pedestrian levels. This arrangement is computationally efficient, but it fails to offer enough accuracy to trust the urban thermal assessment.

The physics-informed mesh (Case 5) serves as the baseline configuration and achieves an MPI=4.00, indicating a stable convergence and high thermal accuracy, but at a higher computational cost. Among all physically meaningful configurations, the optimized mesh (Case 6) has the largest value of MPI (7.14). This mesh combines near-baseline thermal accuracy (0.10% error) with a large reduction in wall-clock time (CI = 0.26) compared to the physics-informed mesh. These findings validate the fact that physics-guided optimization of meshes is the most favourable in balancing accuracy and computational efficiency. Overall, the MPI analysis demonstrates that assigning greater weight to accuracy effectively distinguishes physically reliable mesh configurations from computationally inexpensive but under-resolved solutions. The optimized mesh therefore best satisfies the green computing objective of minimizing energy-to-solution while preserving pedestrian-level thermal fidelity.

The improved performance of the proposed framework compared to conventional mesh refinement approaches can be attributed to the physics-informed mesh distribution strategy adopted in the present study. Unlike uniform mesh refinement techniques, which increase computational cost across the entire domain, the proposed approach selectively concentrates grid resolution in regions characterized by strong flow recirculation, thermal gradients, and near-wall interactions. This enables accurate representation of critical thermal and flow features while avoiding unnecessary refinement in regions with relatively uniform behaviour.

This balance between computation efficiency and numerical accuracy is therefore improved in the present framework and is shown by the improved MPI values obtained for intermediate configuration of meshes. Furthermore, the proposed methodology demonstrates comparable thermal prediction accuracy relative to previously reported urban CFD studies while requiring lower overall mesh density than uniformly refined approaches. In comparison with recent studies employing highly refined meshes or computationally intensive optimization procedures, the present framework offers a computationally efficient alternative without compromising the accuracy of pedestrian-level thermal predictions. Moreover, the proposed method maintains direct physical interpretability, as opposed to emerging data-driven or surrogate-based optimization techniques, which require training data sets and/or reduced-order modelling assumptions.

3.4. Validation of Numerical Model

The validation of the numerical scheme adopted is performed by grid independence study (verification) and comparison with experimental results reported by Uehara et al. [53] Verification ensures that the numerical solution is independent of discretization errors, while validation confirms that the model accurately represents physical reality.

The experimental datasets of Uehara et al. [53] have been widely used in urban microclimate studies and provide detailed measurements of temperature distributions relevant to pedestrian-level thermal environments. [19, 54] The validation simulations employ the same computational domain shown in Figure 2, which is discretized using the same methodology as that of Case 6. To ensure hydrodynamic similitude with experimental setup, the building height, inlet velocity, and surface and inlet temperatures of the domain are scaled according to the experimental configuration of Uehara et al. [53].

The air temperature is evaluated at Point 1, as shown in Figure 2(a), corresponding to the sensor location used in the wind-tunnel experiment. Temperature was evaluated at 11 vertical locations above the ground, at normalized heights of 0.05, 0.1, 0.2, 0.3, 0.4, 0.5, 0.8, 1.0, 1.2, 1.5, and 1.8, consistent with the measurement heights reported in the experimental study [53]. To enable comparison independent of absolute temperature values, the extracted air temperature data are non-dimensionalized using Equation (9), following the normalization approach adopted in previous experimental and numerical studies. 19]

$$\Theta = \frac{T - T_0}{T_s - T_0} \tag{9}$$

where θ is the non-dimensional air temperature and T, T_0 & T_s represents the obtained, reference and surface temperatures, respectively.

The non-dimensional air temperature at 11 vertical heights obtained in the present study was compared with Uehara et al. [53] wind tunnel results (Figure 8(a)). In addition, comparisons were also made with previously published numerical studies by Sen and Roesler [19], Xie et al. [55], and Kim and Baik [56], which have employed similar validation strategies. Figure 8(a) presents the comparison of non-dimensional temperature across all measurement points, while Figure 8(b) provides a zoomed view near the ground.

These results indicate that the numerical model reproduces the typical thermal stratification reported in the

experiment. It has been observed that there is higher temperatures nearby ground surface and a smooth transition towards roof. Overall, a good agreement is observed across most points and specifically near-ground region, which is of the utmost concern to the thermal exposure to pedestrians. There is a minor deviation near the ground, but it is consistent with previous numerical studies.

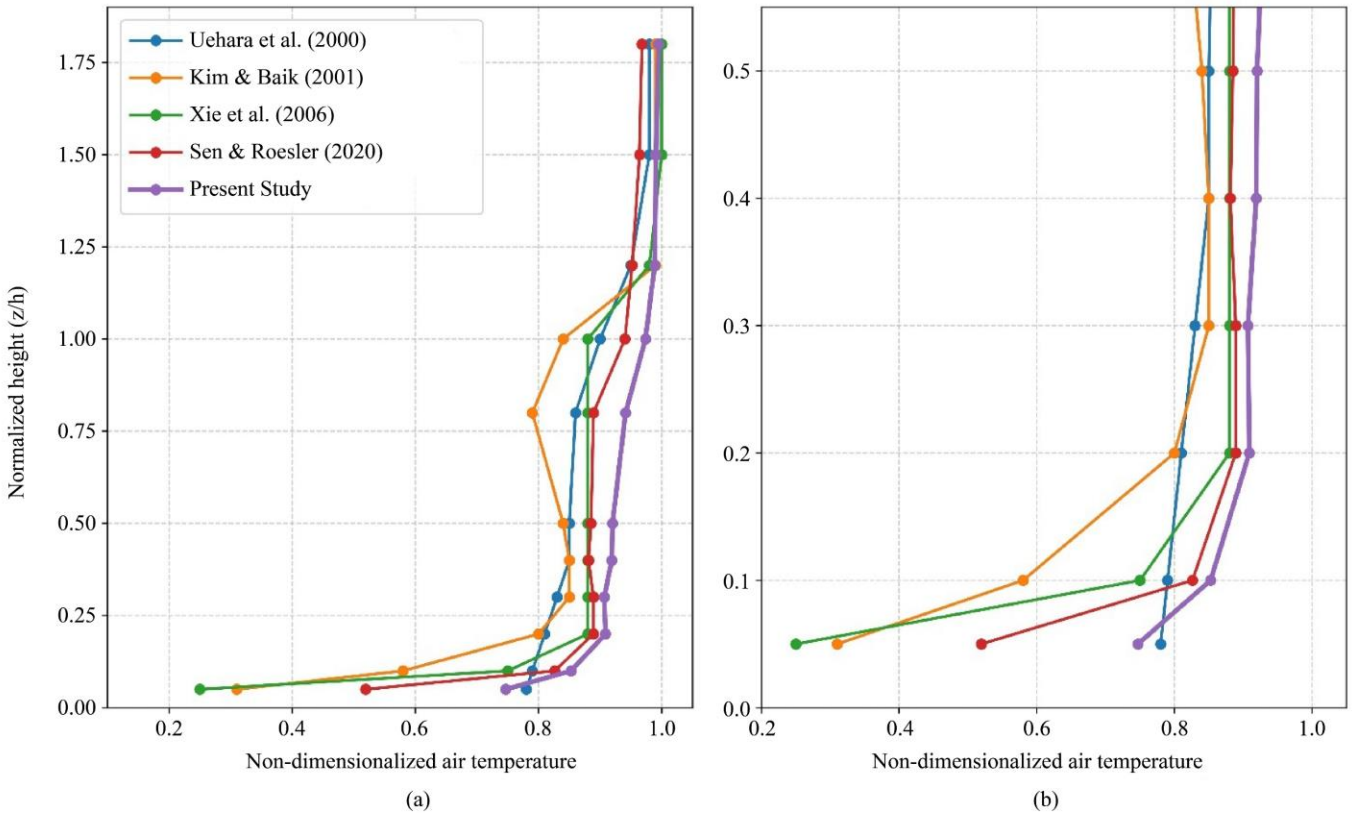

Fig. 8 Comparison of non-dimensional air temperature at Point 1 (along vertical plane) of the present study with wind tunnel data and previous numerical studies, with (a) showing the full-height temperature distribution, & (b) highlighting the near-ground temperature distribution

The non-dimensional temperature profiles were used to calculate error metrics that quantitatively assess the agreement between the numerical predictions and experimental measurements. The Root Mean Square Error (RMSE) and Mean Absolute Error (MAE) between the simulated and experimental data across all the measurement locations are obtained by using Equations (10) and (11), respectively. The obtained MAE and RMSE values were 0.0573 and 0.0634, respectively, which were good agreements between the present simulations and the experimental observations.

$$\mathrm{MAE} = \frac{1}{N}\sum_{i=1}^{N}\left|\theta_i^{\mathrm{sim}} - \theta_i^{\mathrm{exp}}\right| \quad (10)$$

$$\mathrm{RMSE} = \sqrt{\frac{1}{N}\sum_{i=1}^{N}\left(\theta_i^{\mathrm{sim}} - \theta_i^{\mathrm{exp}}\right)^2} \quad (11)$$

The numerical solution is then checked using a grid independence study with meshes with around 0.5 million (coarse), 1 million (medium) and 2 million (fine) elements. The drag coefficients have been tracked at the end of convergence to check for mesh sensitivity. The relative errors for the coarse & medium mesh and medium & fine mesh was determined to be 2.1% and 1.9% respectively, showing that the difference is not that great if the mesh is to be refined further. The numerical results in the above are consistent with the results being approximately grid independent for the selected mesh density.

4. Limitations and Futuristic Directions

The results of this study provide important information on the effects of mesh configuration on the thermal accuracy and computational efficiency of Urban CFD simulations. It is important to note, however, that there are some limitations which will help to explain the scope of work.

The urban domain that was taken in the present study is a simplified, hypothetical urban domain that is meant to isolate mesh-related effects and retain computational tractability. This approach allows the organized comparison of mesh settings, but in practice, urban settings are informal with regard to building geometries, surface material and street geometry that may influence airflow and thermal behaviour in different ways. Therefore, future work should expand this framework to real-world case studies.

The representative boundary condition used in the study is based on the climatic conditions of Rajkot, Gujarat, and a typical worst-case thermal situation. Although this configuration offers a suitable foundation for assessing thermal stress among pedestrians during hot weather environments, the outcomes may vary in other climatic areas with different wind patterns, atmospheric stability and surfaces. Future studies can therefore test the relevance of suggested mesh strategies in other climatic conditions.

The scope of the present study is restricted to the assessment of pedestrian-level thermal behaviour only. However, similar approaches can also be applied in studies focused on urban heat mitigation strategies. Future work should focus on utilizing similar frameworks for analyzing impact of blue or green infrastructure, which often demands highly refined meshes.

The scalability of the proposed framework is another important consideration. Although the present simulations are conducted on an idealized urban domain, the underlying physics-informed mesh refinement strategy can be extended to larger and more complex urban environments. By concentrating refinement only in regions characterized by strong flow and thermal gradients, the framework can reduce unnecessary computational elements compared to uniformly refined meshes. Nevertheless, as domain complexity and physical modelling requirements increase, computational cost may still rise substantially. Therefore, future large-scale applications may benefit from integration with parallel computing or adaptive mesh refinement approaches to further improve scalability and computational efficiency.

Apart from these limitations, there are still research opportunities in the extension of the current framework. The mesh strategies that have been optimised in this paper can be used to assess urban microclimatic conditions in larger and more heterogeneous real-world urban environments. Also, the integration of the emerging methods of data analysis, including artificial intelligence and machine learning techniques, will also assist in forecasting the most efficient mesh distributions and reducing the computational costs. In addition, the suggested Mesh Performance Index (MPI) can also be further extended and experimented on other urban geometries and under different simulations to generate a generalized model on how to balance numerical performance and computational performance during urban CFD modelling.

5. Conclusion

This paper examined the effect of mesh design on the numerical accuracy and computation efficiency of urban CFD simulations in the context of green computing. An imaginary urban domain having nine similar buildings was considered. Six mesh configurations have been compared under the same boundary conditions to assess pedestrian thermal behaviour and the solver's performance.

The results indicate that uniform mesh refinement results in a significant increase in the cost of a calculation, with minimal or no improvement in convergence behaviour or thermal prediction accuracy. Coarse meshes, on the other hand, reduce the computational effort but fail to resolve the thermal gradients on the pedestrian scale adequately. Conversely, physics-informed and optimized non-uniform mesh strategies are more numerically stable and physics consistent thermal predictions.

The MPI evaluations also support these findings as the MPI of optimized mesh is 1.8 to 178.5 times higher than other configurations. Also, the clock time of the optimized mesh is reduced by nearly 74% in comparison to the baseline case. The result proves the usefulness of physics-guided mesh optimization to minimize the energy-to-solution at the expense of useful pedestrian-level thermal prediction.

The findings point to the fact that sustainable urban CFD modelling requires mesh strategies based on physical insights and not on homogeneous refinement only. The suggested assessment scheme and MPI driven evaluation offer an effective method to create computationally effective and thermally stable urban CFD models. The framework can be used in the future to carry out applications in the fields of urban heat islands mitigation, microclimate evaluation, as well as climate-sensitive urbanization.

Declaration of AI-assisted tools

Authors have used a Large language model viz. ChatGPT for improving the clarity and readability of manuscript. After utilizing this, the authors have reviewed and revised the content.

Conflicts of Interest

No conflict of interest that may affect the publication of this paper.

Data Availability

Data can be obtained through a reasonable request to corresponding author.

Funding Statement

No funding received for this work.

References

[1] G.Y. Cao et al., “Urban Growth in China: Past, Prospect, and its Impacts,” *Population and Environment*, vol. 33, pp. 137-160, 2011. [CrossRef] [Google Scholar] [Publisher Link]

[2] Rani Mughal, Javed Manzoor, and Rouf Ahmad Wagay, "Growing Urbanization in the Jammu Province of Jammu and Kashmir, India: an Environmental and Social Interpretation," *Journal of Bioresource Management*, vol. 11, no. 2, pp. 174-185, 2024. [Google Scholar] [Publisher Link]

[3] Arshad Ahmad Lone, G. M. Rather, and M. Sultan Bhat, *Urbanization and Quality of Human Health in Srinagar City, Jammu and Kashmir*, Environment and Health in Jammu and Kashmir and Ladakh, 1st ed., pp. 1-18, 2023. [Google Scholar] [Publisher Link]

[4] Muhammad Waqar Younis, Edore Akpokodje, and Syeda Fizzah Jilani, "Urbanization and its Environmental Impact in Ceredigion County, Wales: A 20-Year Remote Sensing and GIS-Based Assessment (2003–2023)," *Sensors*, vol. 25, no. 17, pp. 1-21, 2025. [CrossRef] [Google Scholar] [Publisher Link]

[5] Kangning Huang et al., "Projecting Global Urban Land Expansion and Heat Island Intensification through 2050," *Environmental Research Letters*, vol. 14, no. 11, pp. 1-12, 2019. [CrossRef] [Google Scholar] [Publisher Link]

[6] Svetlana Vujovic et al., "Urban Heat Island: Causes, Consequences, and Mitigation Measures with Emphasis on Reflective and Permeable Pavements," *CivilEng*, vol. 2, no. 2, pp. 459-484, 2021. [CrossRef] [Google Scholar] [Publisher Link]

[7] Seonju Jang, Jinhyun Bae, and YouJoung Kim, "Street-level Urban Heat Island Mitigation: Assessing the Cooling Effect of Green Infrastructure using Urban IoT Sensor Big Data," *Sustainable Cities and Society*, vol. 100, pp. 1-51, 2024. [CrossRef] [Google Scholar] [Publisher Link]

[8] Sahidul Islam et al., "Urban Heat Island Effect in India: A Review of Current Status, Impact and Mitigation Strategies," *Discover Cities*, vol. 1, pp. 1-28, 2024. [CrossRef] [Google Scholar] [Publisher Link]

[9] Kyeongjoo Park et al., "Changes in Urban Heat Island Intensity with Background Temperature and Humidity and their Associations with Near-surface Thermodynamic Processes," *Urban Climate*, vol. 58, pp. 1-18, 2024. [CrossRef] [Google Scholar] [Publisher Link]

[10] Mehrdad Karimimoshaver, Rezvan Khalvandi, and Mohammad Khalvandi, "The Effect of Urban Morphology on Heat Accumulation in Urban Street Canyons and Mitigation Approach," *Sustainable Cities and Society*, vol. 73, 2021. [CrossRef] [Google Scholar] [Publisher Link]

[11] Hongyuan Huo et al., "Simulation of the Urban Space Thermal Environment Based on Computational Fluid Dynamics: A Comprehensive Review," *Sensors*, vol. 21, no. 20, pp. 1-27, 2021. [CrossRef] [Google Scholar] [Publisher Link]

[12] Xiaoyue Xu, Zhi Gao, and Mingjie Zhang, "A Review of Simplified Numerical Approaches for Fast Urban Airflow Simulation," *Building and Environment*, vol. 234, 2023. [CrossRef] [Google Scholar] [Publisher Link]

[13] Pier Francesco Melani, George Pechlivanoglou, and Alessandro Bianchini, "Using Multi-scale CFD Simulations to Improve Pedestrian Comfort within Built Areas in Complex Terrains," *Journal of Physics: Conference Series: ATI Annual Congress*, Benevento, Italy, vol. 3143, pp. 1-11, 2025. [CrossRef] [Google Scholar] [Publisher Link]

[14] Paulo Ulisses da Silva, Gustavo Bono, and Marcelo Greco, "Assessing Pedestrian Comfort in Dense Urban Areas Using CFD Simulations: A Study on Wind Angle and Building Height Variations," *Fluids*, vol. 10, no. 9, pp. 1-30, 2025. [CrossRef] [Google Scholar] [Publisher Link]

[15] Muhammad Zeeshan, and Zaib Ali, "Heat Stress Mitigation in Urban Streets Having Hot Humid Climatic Conditions: Strategies and Performance Results from a Real Scale Retrofitting Project," *Science and Technology for the Built Environment*, vol. 28, no. 4, pp. 513-526, 2022. [CrossRef] [Google Scholar] [Publisher Link]

[16] Peng Cao, and Wenhui Li, "Evaluation and Optimization of Outdoor Wind Environment in Block Based on Space Syntax and CFD Simulation," *PLoS One*, vol. 19, no. 3, pp. 1-17, 2024. [CrossRef] [Google Scholar] [Publisher Link]

[17] Lup Wai Chew, Negin Nazarian, and Leslie Norford, "Pedestrian-Level Urban Wind Flow Enhancement with Wind Catchers," *Atmosphere*, vol. 8, no. 9, pp. 1-22, 2017. [CrossRef] [Google Scholar] [Publisher Link]

[18] An-Shik Yang et al., "CFD Assessment of Wind Energy Potential: A Combined Framework of Urban Morphology and Design Modification of High-rise Buildings with Voids," *Journal of Wind Engineering and Industrial Aerodynamics*, vol. 271, 2026. [CrossRef] [Google Scholar] [Publisher Link]

[19] Sushobhan Sen, and Jeffery Roesler, "Wind Direction and Cool Surface Strategies on Microscale Urban Heat Island," *Urban Climate*, vol. 31, 2020. [CrossRef] [Google Scholar] [Publisher Link]

[20] José Galindo et al., "Impact of Mesh Resolution and Temperature Effects in Jet Ejector CFD Calculations," *Applied Sciences*, vol. 15, no. 7, pp. 1-19, 2025. [CrossRef] [Google Scholar] [Publisher Link]

[21] W.N.W. Yahya et al., "CFD Simulation on the Pressure Distribution for an Isolated Single-Story House with Extension: Grid Sensitivity Analysis," *IOP Conference Series: Earth and Environmental Science: 4th International Conference on Civil and Environmental Engineering for Sustainability*, Langkawi, Malaysiam, vol. 140, pp. 1-9, 2018. [CrossRef] [Google Scholar] [Publisher Link]

[22] Zhenxing Li et al., "Evaluating the Impact of Road Layout Patterns on Pedestrian-Level Ventilation Using Computational Fluid Dynamics (CFD)," *Atmosphere*, vol. 16, no. 2, pp. 1-19, 2025. [CrossRef] [Google Scholar] [Publisher Link]

[23] Rukiye Cetin, and Ardeshir Mahdavi, "An Empirically-based Assessment of CFD Utility in Urban-level Air Flow Studies," *Proceedings of Building Simulation 2015: 14th Conference of IBPSA*, Hyderabad, India, pp. 796-803, 2015. [CrossRef] [Google Scholar] [Publisher Link]

[24] Francisco Toja-Silva et al., "A Review of Computational Fluid Dynamics (CFD) Simulations of the Wind Flow Around Buildings for Urban Wind Energy Exploitation," *Journal of Wind Engineering and Industrial Aerodynamics*, vol. 180, pp. 66-87, 2018. [CrossRef] [Google Scholar] [Publisher Link]

[25] Ted Stathopoulos et al., "Urban Wind Energy: Some Views on Potential and Challenges," *Journal of Wind Engineering and Industrial Aerodynamics*, vol. 179, pp. 146-157, 2018. [CrossRef] [Google Scholar] [Publisher Link]

[26] Ruoping Chu, and Kai Wang, "CFD in Urban Wind Resource Assessments: A Review," *Energies*, vol. 18, no. 10, pp. 1-21, 2025. [CrossRef] [Google Scholar] [Publisher Link]

[27] Kristina Kostadinović Vranešević et al., "Furthering Knowledge on the Flow Pattern around High-Rise Buildings: LES Investigation of the Wind Energy Potential," *Journal of Wind Engineering and Industrial Aerodynamics*, vol. 226, 2022. [CrossRef] [Google Scholar] [Publisher Link]

[28] Yu-Hsuan Juan et al., "CFD Assessment of Wind Energy Potential for Generic High-rise Buildings in Close Proximity: Impact of Building Arrangement and Height," *Applied Energy*, vol. 321, pp. 1-22, 2022. [CrossRef] [Google Scholar] [Publisher Link]

[29] Yaxing Du, Cheuk Ming Mak, and Zhengtao Ai, "Modelling of Pedestrian Level Wind Environment on a High-Quality Mesh: A Case Study for the HKPolyU Campus," *Environmental Modelling & Software*, vol. 103, pp. 105-119, 2018. [CrossRef] [Google Scholar] [Publisher Link]

[30] Qians Liang et al., "Simulating Microscale Urban Airflow and Pollutant Distributions Based on Computational Fluid Dynamics Model: A Review," *Toxics*, vol. 11, no. 11, pp. 1-14, 2023. [CrossRef] [Google Scholar] [Publisher Link]

[31] B. Blocken, W.D. Janssen, and T. Van Hooff, "CFD Simulation for Pedestrian wind Comfort and Wind Safety in Urban Areas: General Decision Framework and Case Study for the Eindhoven University Campus," *Environmental Modelling & Software*, vol. 30, pp. 15-34, 2012. [CrossRef] [Google Scholar] [Publisher Link]

[32] Yoshihide Tominaga et al., "AIJ Guidelines for Practical Applications of CFD to Pedestrian Wind Environment Around Buildings," *Journal of Wind Engineering and Industrial Aerodynamics*, vol. 96, no. 10-11, pp. 1749-1761, 2008. [CrossRef] [Google Scholar] [Publisher Link]

[33] P.J. Richards, and S.E. Norris, "Appropriate Boundary Conditions for Computational Wind Engineering Models Revisited," *Journal of Wind Engineering and Industrial Aerodynamics*, vol. 99, no. 4, pp. 257-266, 2011. [CrossRef] [Google Scholar] [Publisher Link]

[34] T. Van Hooff, and B. Blocken, "Coupled Urban Wind Flow and Indoor Natural Ventilation Modelling on a High-Resolution Grid: A Case Study for the Amsterdam ArenA Stadium," *Environmental Modelling & Software*, vol. 25, no. 1, pp. 51-65, 2010. [CrossRef] [Google Scholar] [Publisher Link]

[35] Guglielmo Vivarelli, Ning Qin, and Shahrokh Shahpar, "A Review of Mesh Adaptation Technology Applied to Computational Fluid Dynamics," *Fluids*, vol. 10, no. 5, pp. 1-41, 2025. [CrossRef] [Google Scholar] [Publisher Link]

[36] Hanen Amor, and Fayssal Benkhaldoun, "Adaptive Mesh Refinement for Flow and Transport Problem in Heterogeneous Porous Media," *Mathematics and Computers in Simulation*, vol. 239, pp. 766-789, 2026. [CrossRef] [Google Scholar] [Publisher Link]

[37] Amirhossein Fattahi et al., "Measuring Accuracy and Computational Capacity Trade-offs in an Hourly Integrated Energy System Model," *Advances in Applied Energy*, vol. 1, pp. 1-22, 2021. [CrossRef] [Google Scholar] [Publisher Link]

[38] Zohreh Moradinia, Hans Vandierendonck, and Adrian Murphy, "Navigating Speed–Accuracy Trade-Offs for Multi-Physics Simulations," *Meccanica*, vol. 60, pp. 1583-1599, 2025. [CrossRef] [Google Scholar] [Publisher Link]

[39] Aliasghar Azma, and Yakun Liu, "Enhancing CFD Computational Efficiency using Hybrid Data-driven and Physics-based Modeling," *Case Studies in Thermal Engineering*, vol. 78, pp. 1-11, 2026. [CrossRef] [Google Scholar] [Publisher Link]

[40] Xiaotong Luo, Jun Yin, and Simon Kuhn, "Implementation of a Data-driven Model for Mesh-induced Error Corrections in CFD Simulations of Stirred Tanks," *Chemical Engineering Research and Design*, vol. 223, pp. 331-347, 2025. [CrossRef] [Google Scholar] [Publisher Link]

[41] Azfarizal Mukhtar, Ahmad Shah Hizam Md Yasir, and Mohamad Fariz Mohamed Nasird, "A Machine Learning-based Comparative Analysis of Surrogate Models for Design Optimisation in Computational Fluid Dynamics," *Heliyon*, vol. 9, no. 8, pp. 1-19, 2023. [CrossRef] [Google Scholar] [Publisher Link]

[42] Kenza Tlales et al., "Machine Learning Mesh-adaptation for Laminar and Turbulent Flows: Applications to High-Order Discontinuous Galerkin Solvers," *Engineering with Computers*, vol. 40, pp. 2947-2969, 2024. [CrossRef] [Google Scholar] [Publisher Link]

[43] Kheir-Eddine Otmani et al., "Toward a Robust Detection of Viscous and Turbulent Flow Regions using Unsupervised Machine Learning" *Physics of Fluids*, vol. 35, no. 2, 2023. [CrossRef] [Google Scholar] [Publisher Link]

[44] Paulo Sousa, Carlos Veiga Rodrigues, and Alexandre Afonso, "Enhancing CFD Solver with Machine Learning Techniques," *Computer Methods in Applied Mechanics and Engineering*, vol. 429, pp. 1-17, 2024. [CrossRef] [Google Scholar] [Publisher Link]

[45] Sumit Kumar Saurav et al., "Optimization and Scaling of OpenFOAM-based Urban Modeling Simulations," *2024 IEEE International Conference on Electronics, Computing and Communication Technologies (CONECCT)*, Bangalore, India, 2024. [CrossRef] [Google Scholar] [Publisher Link]

[46] Mingyu Yang et al., "Multi-GPU-based Real-time Large-eddy Simulations for Urban Microclimate," *Building and Environment*, vol. 245, 2023. [CrossRef] [Google Scholar] [Publisher Link]

[47] Jumana Abdullah Kareema, and Turkan Ahmed Khaleel, "Green Computing for Sustainability," *Green Technologies and Sustainability*, vol. 4, no. 2, pp. 1-8, 2026. [CrossRef] [Google Scholar] [Publisher Link]

[48] Andrea Pazienza et al., "A Holistic Approach to Environmentally Sustainable Computing," *Innovations in Systems and Software Engineering*, vol. 20, pp. 347-371, 2024. [CrossRef] [Google Scholar] [Publisher Link]

[49] Salil Bharany et al., "A Systematic Survey on Energy-Efficient Techniques in Sustainable Cloud Computing," *Sustainability*, vol. 14, no. 10, pp. 1-89, 2022. [CrossRef] [Google Scholar] [Publisher Link]

[50] Manmeet Singh, and Debra F. Laefer, "Recent Trends and Remaining Limitations in Urban Microclimate Models," *Open Urban Studies and Demography Journal*, vol. 1, pp. 1-12, 2015. [CrossRef] [Google Scholar] [Publisher Link]

[51] Naga Venkata Sai Kumar Manapragada, and Jonathan Natanian, "Urban Microclimate and Energy Modeling: A Review of Integration Approaches," *Sustainability*, vol. 17, no. 7, pp. 1-17, 2025. [CrossRef] [Google Scholar] [Publisher Link]

[52] Jorg Franke et al., "The COST 732 Best Practice Guideline for CFD Simulation of Flows in the Urban Environment: A Summary," *International Journal of Environment and Pollution*, vol. 44, no. 1-4, pp. 419-427, 2011. [CrossRef] [Google Scholar] [Publisher Link]

[53] Kiyoshi Uehara et al., "Wind Tunnel Experiments on How Thermal Stratification Affects Flow in and Above Urban Street Canyons," *Atmospheric Environment*, vol. 34, no. 10, pp. 1553-1562, 2000. [CrossRef] [Google Scholar] [Publisher Link]

[54] Sushobhan Sen, and Lev Khazanovich, "Limited Application of Reflective Surfaces can Mitigate Urban Heat Pollution," *Nature Communications*, vol. 12, pp. 1-8, 2021. [CrossRef] [Google Scholar] [Publisher Link]

[55] Xiaomin Xie, Chun-Ho Liu, and Dennis Y.C. Leung, "Impact of Building Facades and Ground Heating on Wind Flow and Pollutant Transport in Street Canyons," *Atmospheric Environment*, vol. 41, no. 39, pp. 9030-9049, 2007. [CrossRef] [Google Scholar] [Publisher Link]

[56] Jae-Jin Kim, and Jong-Jin Baik, "Urban Street-Canyon Flows with Bottom Heating," *Atmospheric Environment*, vol. 35, no. 20, pp. 3395-3404, 2001. [CrossRef] [Google Scholar] [Publisher Link]